Mon. Not. R. Astron. Soc. **000**, 000–000 (0000) Printed 19 April 2011 (MN LATEX style file v2.2)

Origin and Modelling of Cold Dark Matter Halo Properties: IV. Triaxial Ellipticity

Eduard Salvador-Solé[1] ⋆, Sinue Serra[1], Alberto Manrique[1] and Guillermo González-Casado[2],
[1] *Departament d'Astronomia i Meteorologia, Institut de Ciències del Cosmos (ICC)† Universitat de Barcelona (UB–IEEC), Martí i Franquès 1, E-08028 Barcelona, Spain*
[2] *Dept. Matemàtica Aplicada II, Centre de Recerca d'Aeronàutica i de l'Espai (UPC–IEEC), Universitat Politècnica de Catalunya, E. Omega, Jordi Girona 1–3, E-08034 Barcelona, Spain*

19 April 2011

ABSTRACT
In the three preceding papers in the series, we presented a model dealing with the global and small-scale structure and kinematics of hierarchically assembled, virialised, collisionless systems, which correctly accounted for the typical properties of simulated cold dark matter (CDM) haloes. This model relied, however, on the spherical symmetry assumption. Here we show that the foundations of the model hold equally well for triaxial systems and extend it in a fully accurate way to objects that satisfy the latter more general symmetry. The master equations in the new version take the same form as in the version for spherically symmetric objects, but the profiles of all the physical quantities are replaced by their respective spherical averages. All the consequences of the model drawn under the spherical symmetry assumption continue to hold. In addition, the new version allows one to infer the axial ratios of virialised ellipsoids from those of the corresponding protoobjects. The present results generalise and validate those obtained in Papers I, II and III for CDM haloes. In particular, they confirm that all halo properties are the natural consequence of haloes evolving through accretion and major mergers from triaxial peaks (secondary maxima) in the primordial density field.

Key words: cosmology: cosmology: theory — dark matter — dark matter: haloes — triaxial symmetry — dynamics — self-gravitating systems — galaxies

1 INTRODUCTION

In the three preceding papers in the series, we presented a simple model of the global inner structure (Salvador-Solé et al. 2011a, hereafter Papers I), substructure (Salvador-Solé et al. 2011b, hereafter Paper II) and kinematics (Salvador-Solé et al. 2011c, hereafter Paper III) of virialised collisionless systems grown by pure accretion (PA). Furthermore, the model was shown to also hold for virialised objects that have suffered major mergers, so it is valid for all hierarchically assembled virialised objects, regardless of their aggregation history.

Applied to cold dark matter (CDM) haloes, this model allowed us to show that the roughly universal typical mass density, subhalo number density, pseudo phase-space density, anisotropy and specific angular momentum profiles shown by those objects in numerical simulations (Navarro et al. 1997; Springel et al. 2008; Taylor and Navarro 2001; Hansen and Moore 2006; Bullock et al. 2001; Navarro et al. 2010; see further references in Papers I, II and III) result naturally from the evolution of haloes from peaks (secondary maxima) in the primordial random Gaussian field of density perturbations. There is, however, one important caveat: the model presumed spherical symmetry, while neither haloes nor peaks are strictly spherically symmetric.

Virialised haloes exhibit a substantial triaxial ellipticity at the quadrupole order of approximation, with a trend towards the prolate rather than oblate shape (e.g. Frenk et al. 1988; Dubinski & Carlberg 1991;Warren et al. 1992; Cole & Lacey 1996; Springel et al. 2004; Allgood et al. 2006; Hayashi et al. 2007; Macciò et al. 2007; Stadel et al. 2009). The minor to major axial ratio takes a roughly uniform value of about 0.6, with a slight, still controversial, trend to an outward-decreasing ellipticity (Frenk et al. 1988; Bullock 2002; Jing & Suto 2002; Springel et al. 2004; Kasun &

⋆ E-mail: e.salvador@ub.edu
† Associated with the Instituto de Ciencias del Espacio, Consejo Superior de Investigaciones Científicas

Evrard 2005; Bailin & Steinmetz 2005; Libeskind et al. 2005; Allgood et al. 2006; Hayashi et al. 2007; Bett et al. 2007; Stadel et al. 2009). Likewise, the isodensity contours in the immediate neighbourhood of primordial peaks are also triaxial, even for very high peaks where they tend to be more spherical (Doroshkevich 1970; Bardeen et al. 1986). Unfortunately, there is so far no theoretical model making the link between the triaxiality of haloes and their seeds.

The spherical symmetry assumption was introduced in Paper I in order to facilitate the mathematical treatment and to make the reasoning more transparent. Clearly, the satisfactory results obtained under that assumption suggest that the model, as well as the origin for halo properties mentioned above, must be essentially correct, despite the departure of haloes from spherical symmetry. However, this is not obvious because, as is well known, any small departure from sphericity in the linear initial configuration is dramatically amplified during the non-linear evolution of the system (Zeldovich 1970), which might yield important differences in real triaxial virialised systems compared to the ideal spherical ones. It should therefore be verified that, for triaxial objects: i) the foundations of the model are still well justified, ii) its master equations remain valid; and iii) its consequences for CDM haloes are retained.

In the present paper, we address these issues. We show that ellipsoidal objects that grow by PA develop outwardly by keeping the instantaneous inner region unaltered, just as in the spherically symmetric case, and that the virial radius defined as in spherical objects also gives an accurate measure of the radius enclosing any given mass. Following the prescription by González-Casado et al. (2007), we then show that the same equations for spherically symmetric systems given in Papers I, II and III hold for triaxial systems, simply by replacing the radial profiles of all physical quantities by their respective spherical averages. In addition, the model enables us to calculate the ellipticity of triaxial virialised objects from that of their (real or putative; see Paper I) seeds evolving by PA. Last but not least, we show that all the important consequences of the model for CDM haloes hold for the more general and realistic case of triaxial objects.

The paper is organised as follows. In section 2, we revisit the foundations of the model for triaxial ellipsoids. In section 3, we rebuild the model for such systems. Section 4 is devoted to determining the ellipticity of virialised objects formed from triaxial seeds. The application of the model to CDM haloes is addressed in section 5 and a brief summary is given in section 6.

Throughout the paper we adopt the concordance model with $(\Omega_{\rm m}, \Omega_\Lambda, h, \sigma_8) = (0.3, 0.7, 0.7, 0.9)$. However, we use for simplicity Newtonian dynamics with null cosmological constant. This is enough for CDM haloes but, if we want to be formally consistent, we must simply add $-\Lambda/(8\pi G)$, with G the gravitational constant, to the density where it has the meaning of a gravitational source (not an inertial factor). This means, in practice, to replace everywhere $GM(r)$ by $GM(r) - \Lambda\, r^3/6$. A package with the numerical codes used in the present paper is publicly available from `www.am.ub.es/∼cosmo/haloes&peaks.tgz`.

2 FOUNDATIONS OF THE MODEL

The foundations of the model that we built in the previous papers, justified in Paper I for spherically symmetric systems, were: (i) virialised objects that grow by PA develop from the inside out by keeping the instantaneous inner structure unaltered, and (ii) the radius encompassing a given mass M coincides with the usual virial radius calculated from the energy of the system at turnaround. In what follows, we show that both these statements still hold for triaxial systems.

2.1 Inside-out Growth

In Paper I, it was possible to study the effects of shell-crossing in the virialisation of collisionless systems that undergo PA thanks to the fact that, in spherically symmetric systems, spherical shells conserve their shape throughout the evolution. The gravitational pull on the particles then depends only on their total inner mass. Consequently, by truncating the system at a given spherical shell, the total energy E of that section is conserved as long as it is its inner mass, despite the varying mass distribution of the real (non-truncated) system inside and outside the shell. This allowed us to show that shell-crossing yields a secular energy loss by shells that causes their orbits to contract in an orderly fashion with no apocentre crossing before and after turnaround[1]. As a consequence, the central virialised object necessarily grows from the inside out.

Unfortunately, the shape of shells in ellipsoidal collapse is only conserved (at first-order in the perturbations) during the linear evolution (e.g. Peebles 1980). After turnaround, particles soon fall along non-radial orbits and shells tend to change their shape dramatically (pancake collapse; Zeldovich 1970). In addition, the truncation of the system at any shell of whatever shape is not of much help when it comes to monitoring its evolution, because the particle gravitational energy depends in this case on the whole mass distribution inside and outside the shell. On the other hand, the total energy of a truncated ellipsoid certainly is conserved, but the evolution of this section deviates nonetheless from the one it would undergo embedded in the whole system owing to the different gravitational pull exerted by the outer matter in the two cases. This implies that the simple reasoning followed in Paper I showing that virialised spherically symmetric objects grow in PA from the inside out is not valid for triaxial systems. Nonetheless, the similar way virialisation proceeds in triaxial systems still leads to the same conclusion.

After a shell reaches turnaround, it collapses and rebounds, interacting with other parts of the system. If the particles were to conserve their energy, they would reach the same apocentre after completing one orbit. However, the interaction of particles with other parts of the system causes them to lose some energy, which leads to the virialisation of the system, so the new apocentre locus is somewhat different from the initial one at turnaround. As opposed to what happens in the spherical case, particles do not reach the

[1] The turnaround of particles undergoing PA is defined as their first apocentre.

new locus of null velocity simultaneously. However, as the typical time for particle energy loss or, equivalently, for variation of their null-velocity locus is substantially larger than the orbital period, the apocentre surfaces are well-defined at any given moment despite being possibly traced by particles having completed different numbers of orbits. For symmetry reasons, those apocentre surfaces are also triaxial ellipsoids, as the shell at turnaround, but with different axial ratios and of progressively smaller extent. In other words, the apocentre ellipsoids traced by particles belonging to any ellipsoidal shell at turnaround progressively shrink and change their triaxial ellipticity.

The key point in the reasoning showing that triaxial virialised objects growing by PA also develop inside-out is that, similarly to what happens in the spherical case, the apocentre ellipsoids for different shells at turnaround evolve without crossing each other. Indeed, if two such apocentre ellipsoids coincided at some point, the particles belonging to the two surfaces at that point with identical (null) velocity would describe identical orbits and the shells would not actually cross each other. Therefore, the system contracts orderly without apocentre crossing by conserving the mass inside each apocentre ellipsoidal surface until particles defining that surface no longer lose any significant energy and stabilise their orbits. As apocentre ellipsoids do not cross each other, in particular at the frontier of the instantaneous steady region, when they stop contracting, the central triaxial virialised object grows automatically from the inside out, just as in spherical PA.

The situation is, therefore, essentially the same as in spherically symmetric systems. The only difference is that, in triaxial systems, the gravitational pull suffered by particles comes from matter located inside and outside their radii, meaning that the energy exchange between homoeoids[2] does not proceed through shell-crossing, but it takes place *at a distance* through the change in their respective mass distributions. As mentioned in Paper I, the energy exchange between shells that takes place via shell-crossing does not affect the regions beyond the instantaneous turnaround radius because particles at those radii have not crossed yet other shells. However, owing to the energy exchange at a distance in triaxial systems, the possibility cannot be ruled out in such a case that virialising shells exchange energy with matter beyond the instantaneous ellipsoid at turnaround. If this were the case, the linear theory of structure formation that assumes no coupling among scales would be compromised. (See the discussion on this point for spherical systems in Paper I.) Clearly, the successful predictions of that theory support the idea that there is essentially no energy exchange across the instantaneous ellipsoid at turnaround even in non-spherical collapse. We next show that this is in fact the case to a high degree of accuracy for triaxial ellipsoids formed by PA from triaxial seeds with rather uniform ellipticity.

In Appendix A, it is shown that the potential energy for a truncated sphere of radius R in triaxial systems takes the form

$$W(R) = -4\pi \int_0^R \mathrm{d}r\, r^2\, \langle\rho\rangle(r)\, \frac{GM(r)}{r} \left[1 + \left\langle \frac{\delta\rho}{\langle\rho\rangle}\, \frac{\delta\Phi}{\langle\Phi\rangle} \right\rangle (r)\right], \quad (1)$$

where G is the gravitational constant and $\delta\rho$ and $\delta\Phi$ are the deviations of the local density and gravitational potential from their respective spherical averages $\langle\rho\rangle(r)$ and $\langle\Phi\rangle(r)$. From equation (1) it is clear that, *except for second-order terms* in the departures $\delta\rho/\langle\rho\rangle$ and $\delta\Phi/\langle\Phi\rangle$ from sphericity, the potential energy coincides with that of a spherically symmetric system with the same spherically averaged density, which means that the gravitational potential at a given radius depends only on the total inner mass $M(r)$. Furthermore, as shown in section 5, the ellipticity of virialising regions with no marked radial trend remains essentially unaltered during the process, which implies that the factor within square brackets in the integrand on the right of equation (1) takes the also roughly uniform initial value. Thus, the full gravitational potential of the system truncated at any given radius R depends essentially only on the total inner mass, as in spherically symmetric systems. In these conditions, the same reasoning followed in Paper I now leads to the same conclusion that, in collisionless systems evolving by PA, even if they are triaxial, there is (essentially) no energy exchange across the instantaneous (ellipsoidal) surface at turnaround.

2.2 Virial Radius

In Paper I, it was shown that the inside-out growth of a virialised object undergoing smooth spherical PA implies that the radius R enclosing a given mass M is accurately described by the so-called virial radius.

Indeed, the scalar virial relation for spherically symmetric steady objects (with a central density asymptote less steep than r^{-3}), following from integration out to R of the product $4\pi r^3$ times the Jeans equilibrium equation, takes the form

$$4\pi R^3\, \rho(R)\, \sigma_{\rm r}^2(R) = \int_0^R \mathrm{d}r\, 4\pi\, r^2 \rho(r) \left[\sigma^2(r) - \frac{GM(r)}{r}\right], \quad (2)$$

or simply

$$\frac{2E(R)}{W(R)} = 1 - S(R)\,, \quad (3)$$

where $\rho(r)$, $\sigma(r)$ and $\sigma_{\rm r}(r)$ are respectively the density, total and radial velocity dispersion profiles, $E(R)$ and $W(R)$ are the total and potential energies (the latter with origin at infinity) of the *truncated* sphere with radius R, and $S(R)$ is the corresponding scaled surface pressure term, i.e. the member on the left in equation (2) over the absolute value of $W(R)$. Approximating $W(R)$ by the potential energy of the truncated system *assumed with a uniform inner density profile* so as not to be concerned with the actual unknown inner mass distribution, and $E(R)$ by the total energy $E_{\rm ta}(M)$ of the truncated system enclosing identical mass M at turnaround, equation (3) takes the form

$$R_{\rm vir} = -\frac{3}{10}\frac{GM^2}{E_{\rm ta}(M)}\left[1 - S(R)\right], \quad (4)$$

which defines the virial radius $R_{\rm vir}$. Certainly, E is different from $E_{\rm ta}$ due to the energy dissipated by shells during

[2] A homoeoid is the infinitesimal region between two arbitrarily close ellipsoidal isodensity contours.

virialisation and $\rho(r)$ is not uniform but outwards decreasing. Yet, taking into account the mass and energy conservation for truncated spheres contracting *without crossing each other* from their respective turnaround, it was shown in Paper I that both inaccuracies cancel each other and $R_{\rm vir}$ defined according to equation (4) gives *a completely accurate measure*, despite the severe approximations involved in the derivation, of the radius R encompassing the mass M.

Again, the extension of this result to triaxial systems is not obvious. The virial relation adopts in this case a tensorial form with no explicit radius. Nonetheless, the radius $R_{\rm vir}$ defined according to the relation (4) for the mass M encompassed by R and some modified energy for the truncated sphere of radius R to be specified below still gives a fully accurate measure of R. This result is reached by taking *spherically averaged profiles*, hereafter denoted by angular brackets. Note, however, that the spherically averaged total, radial and (1D) tangential velocity dispersion profiles at r coincide with the respective ordinary dispersions over the corresponding spherical shell, $\sigma(r)$, $\sigma_{\rm r}(r)$, and $\sigma_{\rm t}(r)$, so they do not need angular brackets.

As shown in Appendix A, when the collisionless Boltzmann equation is treated in the same way as for spherically symmetric systems in order to derive the Jeans equilibrium equation, one is led to the exact relation

$$4\pi R^3\langle\rho\rangle(R)\sigma_{\rm r}^2(R)+4\pi\int_0^R {\rm d}r\, r^3\langle\delta\rho\,\partial_{\rm r}(\delta\Phi)\rangle(r) = \int_0^R {\rm d}r\, r^2\,\langle\rho\rangle(r)\left[\sigma^2(r)-\frac{GM(r)}{r}\right], \quad (5)$$

where $\delta\rho$ and $\delta\Phi$ are the local deviations of the density and gravitational potential from their respective spherical averages $\langle\rho\rangle$ and $\langle\Phi_{\rm ta}\rangle$. Thus, by defining the "spherical" potential energy and "spherical" total energy respectively as

$$\mathcal{W}(R)\equiv -4\pi\int_0^R {\rm d}r\, r^2\,\langle\rho\rangle(r)\,\frac{GM(r)}{r}\,, \quad (6)$$

and

$$\mathcal{E}(R)\equiv\int_0^R {\rm d}r\, 4\pi r^2\langle\rho\rangle(r)\left[\frac{\sigma^2(r)}{2}-\frac{GM(r)}{r}\right], \quad (7)$$

that is, exactly as the potential and total energy (with potential origin at infinity) for the truncated sphere of radius R in the *spherically averaged object*, and defining the "spherical" scaled surface term $\mathcal{S}(R)$ as the left hand-side of equation (5) over the absolute value of $\mathcal{W}(R)$, one is led to the relation

$$\frac{2\mathcal{E}(R)}{\mathcal{W}(\mathcal{R})}=1-\mathcal{S}(\mathcal{R})\,, \quad (8)$$

which is formally identical to the scalar virial relation (3) for spherically symmetric objects. Making use of the relation (8) and operating as in the derivation of equation (4), we can define the virial radius of the sphere that encompasses the mass M in a steady triaxial ellipsoid as

$$R_{\rm vir}=-\frac{3}{10}\frac{GM^2}{\mathcal{E}_{\rm ta}(M)}\left[1-\mathcal{S}(\mathcal{R})\right]. \quad (9)$$

Equation (9) is identical to equation (4) defining the virial radius for spherically symmetric objects except for the fact that the total energy $E_{\rm ta}(M)$ of the truncated sphere encompassing the same mass M as the ellipsoid at turnaround is replaced by the spherical counterpart $\mathcal{E}_{\rm ta}(M)$. From now on, the centred sphere that has the same mass as a given ellipsoid is referred to as the "associated" sphere (see App. D for the relationship between its radius R and the semiaxes of the ellipsoid). Note that, as apocentre ellipsoids conserve their mass as they contract, their associated spheres automatically do so, too. Following a proof similar to that in Appendix B of Paper I for spherically symmetric systems, we show in Appendix B that $R_{\rm vir}$ given by equation (9) does indeed yield a completely accurate measure of the radius R encompassing the mass M in triaxial systems[3].

Moreover, the negative signs of both $\mathcal{W}(R)$ and $\mathcal{E}(R)$ quantities (see App. A) imply that $\mathcal{S}(R)$ is necessarily less than one, as for the ordinary scaled surface term in spherically symmetric systems. Consequently, as in those systems, a reasonable estimate for the radius encompassing the mass M is simply given by

$$R=-\frac{3}{10}\frac{GM^2}{\mathcal{E}_{\rm ta}(M)}\,. \quad (10)$$

3 EXTENSION OF THE MODEL TO TRIAXIAL SYSTEMS

Once the foundations of the model developed in Papers I, II and III for spherically symmetric systems formed by PA have been shown to hold for triaxial systems as well, we can extend the model to such systems.

3.1 Smooth Accretion

The mass, total spherical energy, mean angular momentum modulus and specific angular momentum variance (see App. A in Paper III) encompassed by any radius R in a smooth *triaxial* steady object satisfy the relations (see the App. C)

$$M(R)=\int_0^R {\rm d}r\, 4\pi r^2\langle\rho\rangle(r)\,, \quad (11)$$

$$\mathcal{E}(R)=\int_0^R {\rm d}r\, 4\pi r^2\langle\rho\rangle(r)\left[\frac{\sigma^2(r)}{2}-\frac{GM(r)}{r}\right], \quad (12)$$

$$J(R)=\int_0^R {\rm d}r\, 4\pi r^2\langle\rho\rangle(r)\,\langle j\rangle(r) \quad (13)$$

and

$$V(R)=\int_0^R {\rm d}r\, 4\pi r^4\langle\rho\rangle(r)\,\sigma_{\rm t}^2(r)\,, \quad (14)$$

respectively, where $\langle j\rangle(r)$ is the spherically averaged angular momentum profile.

These equations are formally identical to equations (4)–(7) in Paper III from which the model for spherically symmetric objects was built. The only difference is that the profiles $\rho(r)$ and $j(r)$ are now replaced by their respective spherical averages, $\langle\rho\rangle(r)$ and $\langle j\rangle(r)$, and the total ordinary energy $E(R)$ of the truncated sphere of radius R is replaced

[3] This is possible thanks to the lack of energy exchange across the instantaneous ellipsoid at turnaround mentioned above (see App. B).

by its spherical version $\mathcal{E}(R)$. Note that this is equivalent to applying the model of spherically symmetric objects to an ideal system equal to the spherical average of the actual triaxial system. Thus, following the same derivation from equations (11)–(14) as in Paper III, the model developed in that paper (and Papers I and II) is automatically extended to triaxial ellipsoids.

Specifically, differentiating equations (11)–(13), one is led to

$$\langle\rho\rangle(r) = \frac{1}{4\pi r^2}\frac{\mathrm{d}M}{\mathrm{d}r}\,, \tag{15}$$

$$\sigma^2(r) = 2\left[\frac{\mathrm{d}\mathcal{E}/\mathrm{d}r}{\mathrm{d}M/\mathrm{d}r} + \frac{GM(r)}{r}\right], \tag{16}$$

$$\langle j\rangle(r) = \frac{\mathrm{d}J/\mathrm{d}r}{\mathrm{d}M/\mathrm{d}r} \tag{17}$$

and

$$\sigma_{\rm t}^2(r) = \frac{\mathrm{d}V/\mathrm{d}r}{r^2\mathrm{d}M/\mathrm{d}r}\,. \tag{18}$$

In addition, there is the trivial relation

$$\sigma_{\rm r}^2(r) = \sigma^2(r) - 2\sigma_{\rm t}^2(r) \tag{19}$$

between the velocity dispersion components and the usual definition of the velocity anisotropy

$$\beta(r) = 1 - \frac{\sigma_{\rm t}^2(r)}{\sigma_{\rm r}^2(r)} = \frac{1}{2}\left[3 - \frac{\sigma^2(r)}{\sigma_{\rm r}^2(r)}\right]. \tag{20}$$

From equations (15)–(18) it is clear that, if all the functions $M(R)$, $\mathcal{E}(R)$, $J(R)$ and $V(R)$ were known, the spherically averaged structural and kinematic profiles of the steady triaxial object could be readily inferred, which would lead to a fully accurate model for virialised ellipsoids.

Taking into account that, in spherically symmetric systems, the radius R encompassing the mass M coincides with the virial radius given by equation (4), it was shown in Paper I that the so-called dissipation factor, defined as the ratio $D(M) \equiv E(M)/E_{\rm ta}(M)$ between the total energies $E(M)$ and $E_{\rm ta}(M)$ of the truncated spheres with mass $M = M(R)$ in the virialised object and the protoobject at turnaround takes the form

$$\begin{aligned} D(R) &= \frac{5}{6}\left[1 + \int_0^R \frac{\mathrm{d}r}{R}\,\frac{r^4\,\bar{\rho}^2(r)}{R^4\,\bar{\rho}^2(R)}\right] \\ &= \frac{\rho(R)}{\bar{\rho}(R)}\left(1 + \frac{2}{5}\frac{\mathrm{d}\ln\bar{\rho}}{\mathrm{d}\ln R} + \frac{1}{5}\frac{\mathrm{d}\ln D}{\mathrm{d}\ln R}\right)^{-1}, \end{aligned} \tag{21}$$

where $\bar{\rho}(r)$ is the mean density in the virialised object within r. The same derivation can now be followed (see App. B), which leads to exactly the same expression (21) for the ratio between the *spherical* energies of the truncated spheres in the steady object and the protoobject at turnaround,

$$\mathcal{E}(M) = D(M)\mathcal{E}_{\rm ta}(M)\,, \tag{22}$$

with the function D given by equation (21) with $\rho(r)$ replaced by $\langle\rho\rangle(r)$ and $\bar{\rho}(r)$ related to $\langle\rho\rangle(r)$ in the usual way for spherically symmetric systems (eq. [C3] in Paper I)

$$\langle\rho\rangle(r) = \bar{\rho}(r)\left(1 + \frac{1}{3}\frac{\mathrm{d}\ln\bar{\rho}}{\mathrm{d}\ln r}\right). \tag{23}$$

Although the relation (22) stands for the *spherical* energies of the truncated spheres associated with the ellipsoids in the virialised object and at turnaround, the same relation holds for the *ordinary* energies as well. To see this, suppose the ratio between the ordinary energies takes the value $\widetilde{D}(M) = E(M)/E_{\rm ta}(M)$. According to the expression for the total and spherical energies we have

$$\mathcal{E}(M) + \delta\mathcal{E}(M) = \widetilde{D}(M)\left[\mathcal{E}_{\rm ta}(M) + \delta\mathcal{E}_{\rm ta}(M)\right], \tag{24}$$

where $\delta\mathcal{E}(M)$ is the difference between the ordinary and spherical energies, of second order in the deviations from sphericity (see App. A) and the subindex *ta* is for the ellipsoid at turnaround. Given the relation (22), equation (24) can be rewritten in the form

$$\left[D(M) - \widetilde{D}(M)\right]\mathcal{E}_{\rm ta}(M) = \widetilde{D}(M)\delta\mathcal{E}_{\rm ta}(M) - \delta\mathcal{E}(M)\,. \tag{25}$$

The member on the left of equation (25) is of second order in the deviations from sphericity, while that on the right is of 0th order. Consequently, both members must vanish independently, implying

$$D(M) = \widetilde{D}(M) \tag{26}$$

and

$$\delta\mathcal{E}(M) = D(M)\delta\mathcal{E}_{\rm ta}(M)\,. \tag{27}$$

The equality (26) tells us that the dissipation factor $\widetilde{D}(R)$ takes identical value, $D(R)$, as for spherically symmetric systems with $M \equiv M(R)$, given by equation (21). The reader is referred to Paper I for the interesting consequences of the form of the dissipation factor $D(R)$ for triaxial ellipsoids in general.

Contrarily to the energy, the particle angular momentum is not altered by shell-crossing and, if the system is isolated, it cannot be altered by external torques either. Hence, the total angular momentum and specific angular momentum variance are conserved. Moreover, if there is no marked rotation of the ellipsoid axes with radius, the internal tidal torques are also negligible. Thus, as the virialised object grows from the inside out, we are led to the conclusion that the total angular momentum and momentum variance within spheres encompassing any given mass should be conserved from the initial time: $J(M) = J_{\rm ta}(M)$, $V(M) = V_{\rm ta}(M)$.

In PA, the kinematics of protoobjects is dominated by the Hubble bulk flow, meaning that, at any point, the mean rotational and peculiar tangential velocities are small compared to the radial velocity, close to the Hubble velocity. One is therefore tempted to also neglect the final total angular momentum and angular momentum variance. By doing this, the solution of the set of equations (15)–(18) for $J(M) = J_{\rm ta}(M) = 0$, $V(M) = V_{\rm ta}(M) = 0$ and $\mathcal{E}(\mathcal{M}) = D(R)\mathcal{E}_{\rm ta}(M)$, with $M = M(R)$ and $D(R)$ given by equation (21), reduces to solving the following single equation (see Paper III)

$$\begin{aligned} \frac{\mathrm{d}(GM^2)}{\mathrm{d}r} = &\left[\frac{r\,\mathcal{E}_{\rm ta}}{GM^2} - \frac{1}{2D(r)}\left(1 + \frac{5\,r\,\mathcal{E}_{\rm ta}}{3\,GM^2}\right)\right]^{-1} \\ &\times\left[\frac{\mathrm{d}(r\mathcal{E}_{\rm ta})}{\mathrm{d}r} - \mathcal{E}_{\rm ta}\left(1 + \frac{3\,GM^2}{10\,r\,\mathcal{E}_{\rm ta}}\right)\right] \end{aligned} \tag{28}$$

for the density profile $\langle\rho\rangle(r)$. This can be done in the following iterative way. The zeroth-order solution is given by $\langle\rho\rangle(r)$ solution of equation (10), from which we can compute

$D(r)$ (eq. [21]). Equation (28) then leads to the first-order $\langle\rho\rangle(r)$ profile and so on so forth. Once $\langle\rho\rangle(r)$ is known at the wanted accuracy, one can calculate the accurate dissipation factor profile, $D(r)$, and multiply $\mathcal{E}_{\rm ta}(r)$ by it in order to obtain the energy $\mathcal{E}(r)$. Then, by differentiation, we are led (eq. [16]) to the wanted velocity dispersion profile, $\sigma(r)=\sigma_{\rm r}(r)$.

The only complication found in such an extension to triaxial ellipsoids of the model for smooth accretion developed in Paper III concerns the determination of the spherical energy distribution at turnaround, $\mathcal{E}_{\rm ta}(M)$. In spherical PA, $E_{\rm ta}(M)$ coincides with the energy distribution in the protoobject at the initial time. However, this is not the case for ellipsoidal PA. For the reasons explained in section 2.1, neither the total ordinary energy nor the spherical version of it for the truncated ellipsoid or its associated sphere are conserved during the expansion phase of the real (embedded) system undergoing PA. Nonetheless, the properties of the ellipsoid at turnaround can still be calculated in the linear regime from those of the protoobject at the initial time, which allows one to calculate $\mathcal{E}_{\rm ta}(M)$. Note that, after reaching turnaround, shells begin to contract and cross each other, but this does not essentially affect the energy of shells beyond the instantaneous ellipsoid at turnaround (see the discussion in sec. 2.1). As this holds for every ellipsoidal shell at turnaround, both $E_{\rm ta}(M)$ and $\mathcal{E}_{\rm ta}(M)$ can be calculated by integrating over the radius the energy of all the spheres associated with the ellipsoidal shells frozen at their respective turnaround. In particular, taking into account that $\sigma_{\rm ta}(r_{\rm ta})$ is null at turnaround, we can write

$$\mathcal{E}_{\rm ta}(M)=-4\pi\int_0^{R_{\rm ta}}{\rm d}r_{\rm ta}\,r_{\rm ta}^2\langle\rho_{\rm ta}\rangle(r_{\rm ta})\,\frac{GM_{\rm ta}(r_{\rm ta})}{r_{\rm ta}}\,, \qquad (29)$$

where $\langle\rho_{\rm ta}\rangle(r_{\rm ta})$, $\sigma_{\rm ta}(r_{\rm ta})$ and $M_{\rm ta}(r_{\rm ta})$ are the spherical averaged density, velocity dispersion and mass profiles for the system with all the shells frozen at turnaround and $R_{\rm ta}$ is the radius of the sphere associated with the current ellipsoid encompassing the mass M at turnaround.

But things are not that simple. It is true that, for isolated systems, the total angular momentum can be neglected. But, even if the initial angular momentum variance is very small in PA, it cannot be neglected because it is tightly related, in linear perturbation theory, to the protohalo departure from sphericity. The triaxial ellipticity of the protohalo causes indeed particles to collapse along non-radial orbits, which translates into an anisotropic local velocity tensor in the virialised object that supports its triaxial shape. The virialisation process that takes place between those initial and final configurations prevents for formally deriving such a velocity anisotropy directly from the initial conditions. However, following the general although restrictive arguments given in Paper III, the final $\beta(r)$ profile can be related to the deviation from sphericity of the isopotential contours in the virialised object through (eq. [18] of Paper III)

$$\frac{\sigma_{\rm t}^2(r)}{\sigma^2(r)}=\left\langle\left(\frac{\delta\Phi}{\langle\Phi\rangle}\right)^2\right\rangle^{1/2}(r)\,. \qquad (30)$$

As shown in section 4 (and App. D), the departure from sphericity of the isopotential contours can in turn be related to the triaxial ellipticity of the protoobject, so one can nonetheless derive the non-radial infall-driven velocity anisotropy of the virialised object from the ellipticity of the protoobject. Then, inserting this anisotropy in the Jeans equilibrium equation for anisotropic, *spherically averaged*, triaxial systems (eq. A8)[4], one can derive the radial velocity dispersion, $\sigma_{\rm r}(r)$, of the virialised object. Finally, making use of the anisotropy profile, one can derive the tangential component, $\sigma_{\rm t}(r)$.

3.2 Clumpy Accretion

As shown in Paper III, the kinematics of virialised objects arise not only from smooth non-radial infall but also from the effects of small- and large-scale structure neglected in the previous derivation. Indeed, during the initial expansion phase, substructure causes the velocity dispersion of the system to increase relative to that of the ideal smooth isolated system. Likewise, tidal torques by the surrounding large-scale structure cause some angular momentum to develop.

Taking into account that relaxed clumps admit the same model as the global object itself, a recursive procedure based on the model for smooth accretion was developed in Paper III, which accounted for the effects of substructure. The same derivation can be followed in the case of triaxial objects and clumps. One must simply replace all the profiles appearing in that derivation by the corresponding spherical averages and the ordinary total energy by the spherical version of it. The result is

$$\sigma^2(r)=(\sigma^s)^2(r)+\sigma_{\rm C}^2(r) \\ +C^2(r)\left\{\left(1+\frac{{\rm d}\ln C}{{\rm d}\ln r}\right)(\sigma_{\rm IC})_{\rm r}^2[rC(r)]+2(\sigma_{\rm IC})_{\rm t}^2[rC(r)]\right\} \qquad (31)$$

$$\sigma_{\rm t}^2(r)=(\sigma_{\rm t}^s)^2(r)+\sigma_{\rm C}^2(r)+C^2(r)\left\{(\sigma_{\rm IC})_{\rm t}^2[rC(r)]\right\}\,, \qquad (32)$$

where $\sigma^s(r)$ and $\sigma_{\rm t}^s(r)$ are respectively the total and tangential velocity dispersions found in smooth non-radial accretion (see sec. 3.1), $\sigma_{\rm C}$ is the (recursive) 1-D velocity dispersion of particles inside clumps, corrected for the peculiar velocity of the clump, and $(\sigma_{\rm IC})_{\rm r}$ and $(\sigma_{\rm IC})_{\rm t}$ are the mass-independent radial and tangential velocity dispersions in the IC medium at turnaround. (See Paper III for the expression of all these velocity dispersions.)

Similarly, the effect of external tidal torques on the triaxial protohalo during the initial expanding phase were modelled, in Paper III, from the Tidal Torque Theory (Doroshkevich 1970; White 1984), assuming the initial ellipsoid homologous and with non-rotating axes, which is essentially satisfied for CDM haloes (see sec. 5). The result, not only valid, but also better justified for triaxial protoobjects, is

$$\frac{j(r)}{j(R)}\;=\;\left[\frac{M(r)}{M(R)}\right]^{-\frac{n+6}{6}}\left[\frac{C(r)r}{C(R)R}\right]^{\frac{3}{2}}\frac{\mu(r)r_{\rm p}^2(r)}{\mu(R)R_{\rm p}^2(R)}$$

[4] The Jeans equation for anisotropic, spherically averaged triaxial systems is identical to that holding for spherically symmetric systems except for one extra term, equal to the spherical average of $\delta\rho\partial_r\delta\Phi$, which must be added to the gravitational pull at r (see App. A). Such an extra term can also be calculated from the ellipticity of the protoobject (see App. D).

$$\times\frac{-\frac{n+6}{6}+\mu^{-1}(r)+\frac{3}{2}\left(1+\frac{\mathrm{d}\ln C}{\mathrm{d}\ln r}\right)\left(\frac{\mathrm{d}\ln M}{\mathrm{d}\ln r}\right)^{-1}}{-\frac{n+6}{6}+\mu^{-1}(R)+\frac{3}{2}\left(1+\frac{\mathrm{d}\ln C}{\mathrm{d}\ln R}\right)\left(\frac{\mathrm{d}\ln M}{\mathrm{d}\ln R}\right)^{-1}}\,, \quad (33)$$

where $r_{\rm p}(r)$ is given by equations (13) and (14) of Paper I, $\mu(r)$ is a scaled inertia momentum defined in equation (E8) of Paper III, and n is the effective spectral index at the relevant scales of the power spectrum of random Gaussian density fluctuations.

3.3 General Implications

The new version for triaxial systems of the model built in Papers I, II and III for spherically symmetric systems coincides with the original version applied to those ideal objects resulting from the spherical average of the real triaxial objects. In fact, some aspects of the original version of the model related to the existence of a non-null tangential velocity in the protohalo (Paper I) or the effects of non-radial infall and external tidal torques (Paper III) are only properly justified in the case of triaxial symmetry.

Consequently, all the implications of the model drawn in Papers I, II and III under the spherical symmetry assumption are validated in the more general case of triaxial symmetry. In particular, following exactly the same reasoning as in Paper III, we are led to the conclusion that, both in smooth and clumpy non-radial accretion, there is one only virialised object arising by PA from any given triaxial protoobject embedded in some large-scale structure and, conversely, for any given virialised object, characterised by some global inner structure, small-scale substructure, kinematics and, as shown in section 4, triaxial ellipticity, one can always find one triaxial protoobject embedded in the appropriate large-scale structure that leads to it by PA. Such one-to-one correspondence between the initial and final configurations, shown in Papers I, II and III for spherical PA and now extended to triaxial PA, demonstrates that any arbitrary virialised object can be seen as emerging by PA from one appropriate triaxial seed. Consequently, the model for triaxial objects developed above assuming PA holds for all hierarchically assembled virialised objects, regardless of their aggregation history (see Paper I for the implications of this conclusion for the peak formalism).

4 ELLIPTICITY

There is, however, one important property inherent to triaxial systems which could not be addressed by means of the spherical model and can now be treated: the ellipticity of the system itself. To specify such an ellipticity we will use the primary and secondary eccentricities, respectively defined from the ellipsoid semiaxes $a \geqslant b \geqslant c$ as

$$e_{\rm p} = \left(1-\frac{c^2}{a^2}\right)^{1/2} \quad (34)$$

and

$$e_{\rm s} = \left(1-\frac{b^2}{a^2}\right)^{1/2} \quad (35)$$

and related to the radius R of the associated sphere through equation (D19).

To derive the eccentricities of the virialised object from those of the protoobject we must take into account that the mass enclosed by the ellipsoid apocentres (or their associated spheres) remains constant as they contract from turnaround (sec. 2.1). The condition $M(R) = M(R_{\rm ta})$ leads to

$$4\pi\, a(R)\, b(R)\, c(R)\, \bar{\rho}(R) = 4\pi\, a(R_{\rm ta})\, b(R_{\rm ta})\, c(R_{\rm ta})\, \bar{\rho}_{\rm ta}(R_{\rm ta})\,. \quad (36)$$

Taking into account equation (23) and the relation (eq. [B2] in Paper III)

$$\langle\rho_{\rm ta}\rangle(R_{\rm ta}) = \frac{\langle\rho\rangle(R)}{C^3(R)}\left(1+\frac{\mathrm{d}\ln C}{\mathrm{d}\ln R}\right)^{-1} \quad (37)$$

between the spherically averaged density at turnaround and in the virialised object, where $C(R) \equiv R_{\rm ta}(R)/R$ is the contraction factor undergone by the shell from turnaround (see Paper III), equation (36) adopts after some algebra the form

$$\frac{(1-e_{\rm p}^2)(1-e_{\rm s}^2)}{[1+(1-e_{\rm p}^2)+(1-e_{\rm s}^2)]^3}(R) = \frac{(1-e_{\rm p}^2)(1-e_{\rm s}^2)}{[1+(1-e_{\rm p}^2)+(1-e_{\rm s}^2)]^3}(R_{\rm ta})\,. \quad (38)$$

Equation (38) is obviously not enough to determine the two eccentricities $e_{\rm p}$ and $e_{\rm s}$ in the final virialised object from those at turnaround. One more equation is needed, which is provided by the relationship between the total energies of the truncated spheres associated with the ellipsoids in the final steady object and at turnaround.

As mentioned, the energy dissipation during virialisation takes place through the exchange at a distance of potential energy between homoeoids as their mass distribution varies. The relation (22) between the spherical energies contains no information regarding the ellipticity of the system[5], but the total ordinary energies $E(M)$ and $E_{\rm ta}(M)$ do. Thus, the relation we need is equation (24), or directly equation (27), relating the differences $\delta\mathcal{E}(M) = E(M) - \mathcal{E}(M)$ and $\delta\mathcal{E}_{\rm ta}(M) = E_{\rm ta}(M) - \mathcal{E}_{\rm ta}(M)$. This latter relations takes the explicit form

$$\int_0^R \mathrm{d}r\, r^2\, \langle\rho\rangle(r)\, \langle\Phi\rangle(r) \left\langle \frac{\delta\rho}{\langle\rho\rangle}\frac{\delta\Phi}{\langle\Phi\rangle}\right\rangle(r) = D(R) \times \int_0^{R_{\rm ta}(R)} \mathrm{d}r_{\rm ta}\, r_{\rm ta}^2\, \langle\rho_{\rm ta}\rangle(r_{\rm ta})\langle\Phi_{\rm ta}\rangle(r_{\rm ta}) \left\langle \frac{\delta\rho_{\rm ta}}{\langle\rho_{\rm ta}\rangle}\frac{\delta\Phi_{\rm ta}}{\langle\Phi_{\rm ta}\rangle}\right\rangle(r_{\rm ta})\,. \quad (39)$$

Differentiating this relation and making use of the contraction factor $C(r)$, we arrive at

$$\left\langle \frac{\delta\rho}{\langle\rho\rangle}\frac{\delta\Phi}{\langle\Phi\rangle}\right\rangle(r) = D(r)\,\frac{\langle\Phi\rangle_{\rm ta}[C(r)r]}{\langle\Phi\rangle(r)} \times \left\langle \frac{\delta\rho_{\rm ta}}{\langle\rho_{\rm ta}\rangle}\frac{\delta\Phi_{\rm ta}}{\langle\Phi_{\rm ta}\rangle}\right\rangle[C(r)r]\,. \quad (40)$$

Equation (40) can also be used to infer the nth-order radial derivative of the mean dimensionless density-potential crossed fluctuation over spheres in the final virialised object

[5] The spherical energy and the mass are related with each other through equation (9) with $\mathcal{S}$ neglected, which means that the previous condition of the equality between the masses encompassed by the associated spheres automatically implies the equality between those spherical energies.

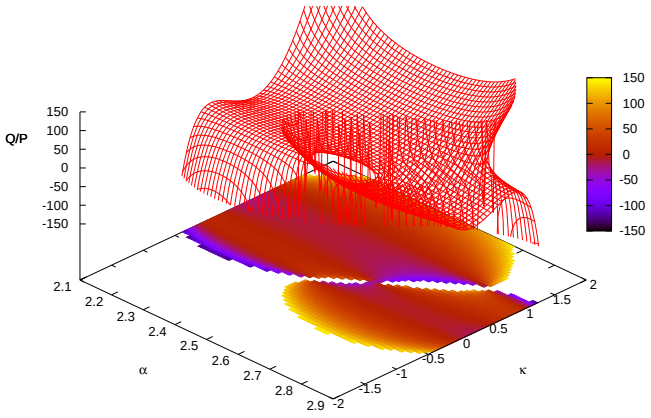

Figure 1. Predicted Q/P ratio between the rms dimensionless density and potential fluctuation fluctuation profiles in self-similar objects with κ the power index of the rms dimensionless density and potential fluctuations and $-\alpha$ that of the spherically averaged density profile.

from identical quantity in the toy object with frozen shells at turnaround.

In Appendix D, the mean dimensionless density-potential crossed fluctuation over spheres of varying radii is related to the squared dimensionless density fluctuation over those spheres, which in turn is related to the eccentricities of the associated ellipsoids through

$$\left\langle \left(\frac{\delta\rho}{\langle\rho\rangle} \right)^2 \right\rangle = -\frac{2}{5} \times \left\{ 1 - \frac{3[(1-e_{\rm p}^2)^2(1-e_{\rm s}^2)^2 + (1-e_{\rm p}^2)^2 + (1-e_{\rm s}^2)^2]}{[(1-e_{\rm p}^2)(1-e_{\rm s}^2) + (1-e_{\rm p}^2) + (1-e_{\rm s}^2)]^2} \right\} . \quad (41)$$

Therefore, taking into account the relation (40), the eccentricities of the virialised object can be readily related to those of the protoobject for the ellipsoid encompassing identical mass. This relation is

$$U(R) \left\{ 1 - \frac{3[(1-e_{\rm p}^2)^2(1-e_{\rm s}^2)^2 + (1-e_{\rm p}^2)^2 + (1-e_{\rm s}^2)^2]}{[(1-e_{\rm p}^2)(1-e_{\rm s}^2) + (1-e_{\rm p}^2) + (1-e_{\rm s}^2)]^2} \right\}_R = \left\{ 1 - \frac{3[(1-e_{\rm p}^2)^2(1-e_{\rm s}^2)^2 + (1-e_{\rm p}^2)^2 + (1-e_{\rm s}^2)^2]}{[(1-e_{\rm p}^2)(1-e_{\rm s}^2) + (1-e_{\rm p}^2) + (1-e_{\rm s}^2)]^2} \right\}_{R_{\rm ta}} . \quad (42)$$

Under the assumption that the ellipsoid axes do not rotate and the rms dimensionless density fluctuation profile is a power-law with index κ, $\langle(\delta\rho/\langle\rho\rangle)^2\rangle^{1/2} = Qr^\kappa$, and adopting the origin of $\langle\Phi\rangle(R)$ and $\langle\Phi\rangle(R_{\rm ta})$ according to equation (A14), the function $U(r)$ takes the form

$$U(R) \equiv \frac{C(R)}{D(R)} \times \frac{1 - \xi_{\rm ta}(R_{\rm ta})\gamma_{\rm ta}(R_{\rm ta})\left\{1 - [1+2\kappa_{\rm ta}]\gamma_{\rm ta}(R_{\rm ta}) - \frac{{\rm d}\ln\gamma_{\rm ta}}{{\rm d}\ln R_{\rm ta}}\right\}}{1 - \xi(R)\gamma(R)\left\{1 - [1+2\kappa]\gamma(R) - \frac{{\rm d}\ln\gamma}{{\rm d}\ln R}\right\}} , \quad (43)$$

where $\xi_{\rm x}(R_{\rm x})$ is defined as $\bar\rho_{\rm x}(R_{\rm x})/[3\langle\rho_{\rm x}\rangle(R_{\rm x})]$ and $\gamma_{\rm x}(R_{\rm x})$ is the logarithmic derivative of the mean dimensionless density-potential crossed fluctuation, with subindex x taking no value or the value "ta" depending on whether the quantity refers to the virialised object or the toy object with shells frozen at turnaround.

As the axial ratios of ellipsoids encompassing a given mass are conserved during the linear expansion phase of PA, the eccentricities at turnaround are identical to those found at the radius encompassing identical mass in the protoobject. In other words, the ellipticity of a virialised object grown by PA can be derived directly from that of the protoobject. Note that the ellipticities at turnaround and in the final virialised object include the effects of any non-null angular momentum[6], while that of the initial protoobject involves no such an effect because the initial protoobject does not essentially rotate. There is no contradiction, however, in this result: during the linear expansion phase, the shape (ellipticity) of the protoobject remains unaltered only at the leading order in the perturbed quantities used in TTT to compute the angular momentum acquired by the system due to external tidal torques (see Paper III and references therein).

In Appendix D, we calculate the relation between the rms dimensionless density and potential fluctuation profiles in the self-similar case, that is when all the (spherically averaged) profiles are power-laws. The result is that both rms dimensionless fluctuation profiles necessarily have identical power index κ. This does not mean that the isodensity and isopotential contours are equally aspherical at any given radius: the height of the rms dimensionless density and potential fluctuation profiles, respectively given by the proportionality factors Q and P, are different in general. Specifically, for an object with spherically averaged density profile $\langle\rho\rangle(r) \propto r^{-\alpha}$, the ratio Q/P depends on κ and α in the following way

$$\frac{Q}{P} = \left[1 - \frac{(1-\alpha)(\kappa-1)\kappa}{(2-\alpha)(3-\alpha)} \right] \times \left(1 - \frac{\frac{3\kappa}{2}\left\{ 1 - \frac{(\kappa-1)}{(2-\alpha)}\left[1 - \frac{(\kappa-2)}{(3-\alpha)} \right] \right\}}{5 - 2\alpha + \kappa/2} \right) . \quad (44)$$

Figure 1 shows the ratio Q/P that results for α in the range $2 < \alpha < 3$ and κ ranging from -2 to 2. The function is well-behaved everywhere except in a narrow strip along the line $\kappa = 5 - 2\alpha$ where it tends to diverge with unphysical negative values. For all values of κ below this strip, Q/P is always larger than one, while above that line it takes values larger than one only far enough from it. As shown in Paper I, α is smaller than 2.5 in self-similar objects, where there is no solution for negative values of κ. Thus, in such objects, the ellipticity is necessarily outwards increasing and the isopotential contours are more spherical than the isodensity contours, which is achieved for large enough values of κ.

[6] The rotational kinetic energy of the truncated sphere is included, indeed, through $\sigma_{\rm ta}$ (σ) within $E_{\rm ta}$ (E).

5 APPLICATION TO CDM HALOES

The model developed in Papers I, II and III yielded very satisfactory predictions for the structural and kinematic profiles of spherically symmetric CDM haloes, regardless of their individual aggregation history. The results obtained in sections 2 and 3 of the present paper show that this was not due to an oversimplification of the problem due to the spherical symmetry assumption. The model holds accurately for the *spherically averaged* profiles (those numerical simulations explicitly refer to) for triaxial systems. On the other hand, the peak trajectory formalism (Manrique & Salvador Solé, 1995,1996; Manrique et al. 1998), used in those papers to relate explicitly the typical halo profiles to the spectrum of primordial density fluctuations in a given hierarchical cosmology, takes into account, through the parameters q and δ_c in equations (21) and (22) of Paper I, that peaks are slightly triaxial and hence do not evolve by spherical PA. Consequently, the present model explains the properties of simulated CDM haloes as the natural result of their evolution through accretion and major mergers from triaxial peaks (secondary maxima) in the primordial random Gaussian density field, as put forward in Papers I, II and III under the spherical approximation.

But, apart from confirming the results derived in those papers, the present extension of the model to triaxial systems should also enable us to infer the typical ellipticity of haloes from that of their seeds. Specifically, taking into account that haloes arise from the evolution by PA of the density field at the *immediate vicinity* of peaks, to characterise the ellipticity including its radial behaviour of haloes, we need to know the spatial derivatives of the density field at the central maximum. Given the random Gaussian behaviour of the primordial density field, their determination is feasible. Unfortunately, the only spatial derivatives at peaks so far determined are the second-order ones characterising the typical eccentricity of isodensity ellipsoids around peaks (Doroshkevich 1970; Bardeen et al. 1986). The third-order spatial derivatives characterising the radial behaviour of this ellipticity (i.e. whether or not the axes rotate with increasing radius and the value of the radial derivative of the typical dimensionless density fluctuation profile) have not yet been determined. As shown in section 4, this is mandatory in order to accurately determine the shape of the final ellipsoids. Nonetheless, we can still have a good idea of this shape.

Indeed, except for the factor $U(R)$, equation (41) takes the form of an identity relation just as equation (38). Consequently, if $U(R)$ were close to one, the final eccentricities would necessarily be close to the initial ones. Interestingly, the set of algebraic equations (38) and (41) can be solved for only a very narrow range of $U(R)$ values around unity. This is shown in Figure 2, where we plot the solution space for varying values of U inferred by means of the practical solving procedure provided in Appendix D. We therefore conclude that, disregarding the actual properties of the ellipsoids in peaks, the final eccentricities are necessarily close to the initial ones. The ratio between the major and minor axes (the major and intermediate axes) in peaks is about 1.7 (1.3) (BBKS)[7], which corresponds to a typical value of

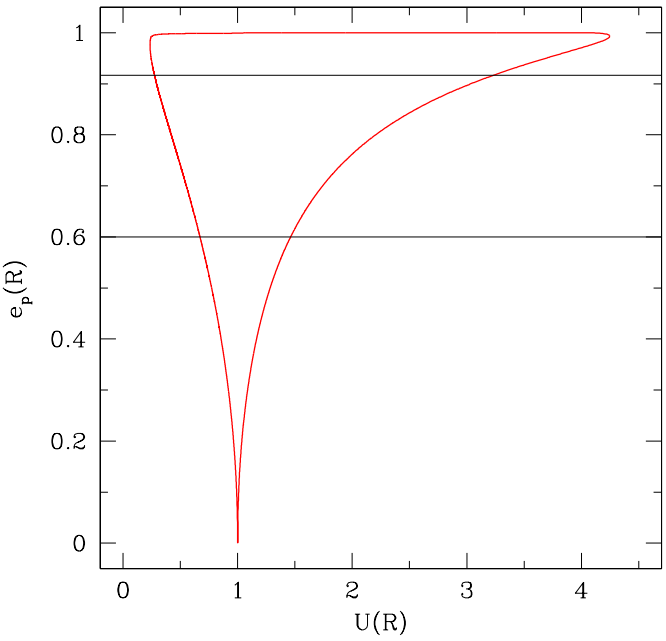

Figure 2. Ellipticity space, delimited by the curve for the primary eccentricity $e_p(R)$ (solid red line), for current CDM haloes with arbitrary mass in the concordance model as a function of the quantify $U(R)$ defined in equation (43). The two horizontal black lines represent the extreme values for e_p corresponding to the extreme axial ratios of simulated haloes reported in the literature.

e_p (e_s) of about 0.81 (0.64). Actually, as the value of $U(R)$ for small R is between one and two, we expect a value of e_p (e_s) in haloes slightly larger than that, typically about 0.9 (0.82), that is closer to the upper values found in numerical simulations (Frenk et al. 1988; Bullock 2002; Jing & Suto 2002; Springel et al. 2004; Kasun & Evrard 2005; Bailin & Steinmetz 2005; Libeskind et al. 2005; Allgood et al. 2006; Hayashi et al 2007; Bett et al. 2007; Stadel et al. 2009).

We can still go a little further. As shown in Appendix D, the ellipsoids cannot be strictly non-rotating and homologous, $\gamma_x(R_x) = 0$, in the protohalo and the virialised halo at the same time. For this to happen, $C(r)/D(r)$ should be constant, while for the typical NFW (or Einasto) $\rho(r)$ profile with the typical mass-concentration relation, this function shows a moderate outward-increasing trend from one to two and it is only constant close to the centre. This conclusion is also consistent with the results of numerical simulations indicating that the ellipticity in haloes is nearly homologous although, near to the edge of the system, the isodensity contours become somewhat more spherical (e.g. Jing & Suto 2002; Bailin & Steinmetz 2005; Allgood et al. 2006; Stadel et al. 2009).

Moreover, as shown in Appendix D, for outer asymptotic power-law profiles, the power indexes of the rms dimensionless density and potential fluctuation profiles coincide. As for the self-similar case studied above, the more or less aspherical behaviour of the isodensity and isopotential contours depends on the index κ and the asymptotic logarithmic

[7] These values are for the standard CDM model. However, at high-redshifts, the cosmological constant goes unnoticed.

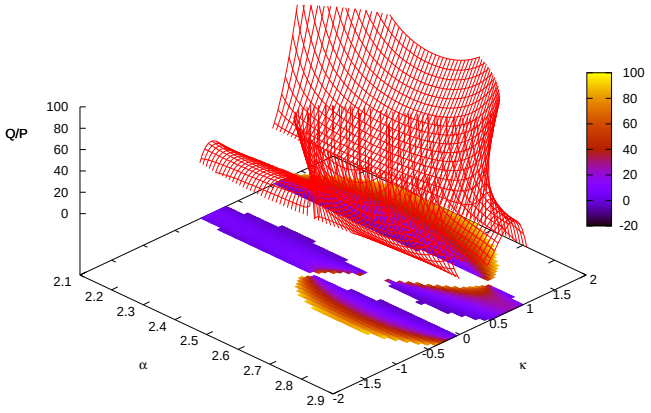

Figure 3. Same as Figure 1 for asymptotic power-law regimes with the range of κ and α indexes leading to only moderate values of Q/P as found in numerical simulations.

slope $-\alpha$ of the density profile. For values of α approaching to 3 as found in virialised haloes[8], the only possible negative values of κ leading to an outwards decreasing ellipticity and to isopotential contours moderately more spherical than the corresponding isodensity contours as found in numerical simulations (Springel et al. 2004; Kasun & Evrard 2005; Hayashi et al. 2007) are found in the quite limited range $-0.2 \lesssim \kappa < 0$ (see Fig. 3). This was used in Paper III to constrain the velocity anisotropy profile.

6 SUMMARY AND CONCLUSIONS

The model developed in Papers I, II and III for the structure (density profile, subhalo abundance and number density profile) and kinematics (pseudo phase-space density, velocity anisotropy and specific angular momentum profiles) of spherically symmetric, hierarchically assembled, virialised, collisionless systems can be extended to triaxial ellipsoids. Its foundations given in Paper I are well justified, indeed, for triaxial systems and the master equations of the model are strictly valid for such systems by simply replacing the radial profiles of the different quantities by their respective spherical averages.

In addition, the present extended version of the model allows one to calculate the ellipticity of virialised objects formed by PA from that of their seeds, the contraction suffered by the sphere associated with any given ellipsoidal isodensity contour at turnaround and the energy loss that goes together with that contraction during virialisation.

With the present results, the model developed over this series of papers explains the origin of the typical, roughly universal, properties shown by virialised CDM haloes in cosmological simulations. These properties are the natural consequence of haloes evolving, through minor and major mergers, from triaxial peaks in the primordial density field. As a byproduct, the model confirms the validity of the peak trajectory formalism for structure formation, which allows one to calculate the typical spherically averaged halo profiles and ellipticity from the spectrum of the primordial density perturbations. As mentioned in the preceding papers, the peak trajectory formalism can be very useful for modelling halo properties on different environments.

[8] As an asymptotic logarithmic slope, α can be larger than the maximum value equal to 2.5 for self-similar objects.

ACKNOWLEDGEMENTS

This work was supported by the Spanish DGES AYA2006-15492-C03-03 and AYA2009-12792-C03-01. One of us, SS, was beneficiary of a grant from the Institut d'Estudis Espacials de Catalunya.

REFERENCES

Allgood B., Flores R.A., Primack J.R., Kravtsov A.V. Wechsler R.H., Faltenbacher A., Bullock J.S. 2006, MNRAS, 367, 1781
Bailin J. & Steinmetz M. 2005, ApJ, 627, 647
Bardeen J. M., Bond J. R., Kaiser N., Szalay, A. S. 1986, ApJ, 304, 15
Bett P., Eke V., Frenk C. S., Jenkins A., Helly J., Navarro J. 2007, MNRAS, 376, 215
Binney J. & Tremaine S. D. 1987, *Galactic dynamics*, Princeton University Press
Bryan G.L. & Norman M. L. 1998, ApJ, 495, 80
Bullock J. S. 2002, in *The shapes of galaxies and their dark haloes*, ed. P. Natarajan, Singapore: World Scientific, 109
Bullock J. S., Dekel A., Kolatt T. S., Kravtsov A. V., Klypin A. A., Porciani C., Primack J. R. 2001, ApJ, 555, 240
Cole S. & Lacey C. 1996, MNRAS, 281, 716
Doroshkevich A. 1970, Astrofizika, 6, 581
Dubinski J. & Carlberg R. G. 1991, ApJ, 378, 496
Frenk C.S., White S.D.M., Davis M., Efstathiou G. 1988, ApJ, 327, 507
González-Casado G., Salvador-Solé E., Manrique A., Hansen S. H. 2007 [arXiv: astro-ph/0702368]
Hansen S. H. & Moore B. 2006, New Astronomy, 11, 333
Hayashi E., Navarro J.F., Springel V. 2007, MNRAS, 377, 50
Jing Y.P. & Suto Y., 2002 ApJ, 574, 538
Kasun S. F. & Evrard A. E. 2005, ApJ, 629, 781
Libeskind N. I., Frenk C. S., Cole S., Helly J. C., Jenkins A., Navarro J. F., Power C. 2005, MNRAS, 363, 146
Macciò A. V., Dutton A. A., van den Bosch F. C., Moore B., Potter D., Stadel J. 2007, MNRAS, 378, 55
Manrique A. & Salvador-Sole E. 1995, ApJ, 453, 6 (MSSa)
Manrique A. & Salvador-Sole E. 1996, ApJ, 467, 504 (MSSb)
Manrique A., Raig A., Solanes J. M., González-Casado G., Stein, P., Salvador-Solé E. 1998, ApJ, 499, 548
Navarro J. F., Frenk C. S.& White S. D. M. 1997, ApJ, 490, 493
Navarro J. F., Ludlow, A., Springel, V., Wang J., Vogelsberger M., White, S. D. M., Jenkins A. R., Frenk, C. S., Helmi A. 2010, MNRAS, 402, 21
Peebles P.J.E. 1980, *The Large-Scale Structure of the Universe*, Princeton University Press
Salvador-Solé E., Manrique A., Serra S. 2011a, submitted to MNRAS, (Paper I)
Salvador-Solé E., Serra S., Manrique A. 2011b, submitted to MNRAS, (Paper II)
Salvador-Solé E., Serra S., Manrique A. 2011c, submitted to MNRAS, (Paper III)

Springel V., White S. D. M., Hernquist L. 2004, IAU Symposium, 220, 421
Springel V. et al. 2008, MNRAS, 391, 1685
Stadel J., Potter D., Moore B., Diemand J., Madau P., Zemp M., Kuhlen M., Quilis V. 2009, MNRAS, 398, L21
Taylor J. E. & Navarro J. F. 2001, ApJ, 563, 483
Warren M. S., Quinn P. J., Salmon J. K., Zurek W. H. 1992, ApJ, 399, 405
White S. D. M. 1984, ApJ, 286, 38
Zeldovich Ya. B. 1970, A&A, 5, 84

APPENDIX A: ORDINARY AND SPHERICAL ENERGIES IN TRIAXIAL SYSTEMS

As well-known, the phase-space density $f(\mathbf{r},\mathbf{v})$ for a virialised collisionless system satisfies the Vlasov equation, that is, the steady collisionless Boltzmann equation coupled with the Poisson equation. Writing the steady collisionless Boltzmann equation in spherical coordinates (e.g. eq. [4p-2] in Binney & Tremaine 1987), multiplying it by the radial velocity $v_{\rm r}$, and integrating over velocity and solid angle, one is led, in the general case of triaxial symmetry, to the following first order differential equation

$$\frac{{\rm d}(\langle\rho\rangle\sigma_{\rm r}^2)}{{\rm d}r}+\frac{\langle\rho\rangle(r)}{r}[3\sigma_{\rm r}^2(r)-\sigma^2(r)] = -\frac{1}{4\pi}\int_0^{2\pi}{\rm d}\varphi\int_0^{\pi}{\rm d}\theta\ \sin\theta\ \rho(r,\theta,\varphi)\,\partial_{\rm r}\Phi(r,\theta,\varphi)\,, \quad \text{(A1)}$$

where $\partial_{\rm r}$ stands for radial partial derivative,

$$\sigma^2(r)=\frac{1}{4\pi\langle\rho\rangle}\int_0^{2\pi}{\rm d}\varphi\int_0^{\pi}{\rm d}\theta\ \sin\theta\int{\rm d}^3v\,v^2\,f(\mathbf{r},\mathbf{v}) = \sigma_{\rm r}^2(r)+2\sigma_{\rm t}^2(r) \quad \text{(A2)}$$

and

$$\rho(r,\theta,\varphi)=\int{\rm d}^3v\,f(\mathbf{r},\mathbf{v})\,. \quad \text{(A3)}$$

To derive equation (A1), it is only needed such conventional assumptions as the continuity in real space of the local density and mean velocities and the fact that f vanishes for large velocities.

Splitting the local density and gravitational potential as

$$\rho(r,\theta,\varphi) = \langle\rho\rangle(r)+\delta\rho(r,\theta,\varphi) \quad \text{(A4)}$$
$$\Phi(r,\theta,\varphi) = \langle\Phi\rangle(r)+\delta\Phi(r,\theta,\varphi)\,, \quad \text{(A5)}$$

and taking into account that the spherically averaged gravitational potential,

$$\langle\Phi\rangle(r)=\frac{1}{4\pi}\int_0^{2\pi}{\rm d}\varphi\int_0^{\pi}{\rm d}\theta\ \sin\theta\,\Phi(r,\theta,\varphi), \quad \text{(A6)}$$

satisfies, by the Gauss theorem, the usual Poisson integral relation for spherically symmetric systems

$$\frac{{\rm d}\langle\Phi\rangle(r)}{{\rm d}r}=\frac{GM(r)}{r^2}, \quad \text{(A7)}$$

equation (A1) adopts the form

$$\frac{{\rm d}(\langle\rho\rangle\sigma_{\rm r}^2)}{{\rm d}r}+\frac{\langle\rho\rangle(r)}{r}[3\sigma_{\rm r}^2(r)-\sigma^2(r)] = -\langle\rho\rangle(r)\frac{GM(r)}{r^2}-\langle\delta\rho\,\partial_{\rm r}(\delta\Phi)\rangle(r)\,. \quad \text{(A8)}$$

Except for the second term on the right, equation (A8) looks exactly as the classical Jeans equation for spherically symmetric systems with anisotropic velocity tensor. Thus, multiplying (A8) by $4\pi r^3{\rm d}r$ and integrating over r, the same steps leading to the scalar virial relation for a spherically symmetric system now lead to

$$4\pi R^3P(R)-2K = -\int_0^R{\rm d}M(r)\frac{GM(r)}{r} -4\pi\int_0^R{\rm d}r\,r^3\langle\delta\rho\,\partial_{\rm r}(\delta\Phi)\rangle\,, \quad \text{(A9)}$$

where

$$P(R)=\langle\rho\rangle(R)\sigma_{\rm r}^2(R) \quad \text{(A10)}$$

is the spherically averaged radial boundary pressure, and

$$K(R)=2\pi\int_0^R{\rm d}r\,r^2\langle\rho\rangle(r)\sigma^2(r) \quad \text{(A11)}$$

is the kinetic energy within R. On the other hand, the total potential energy is

$$W(R) = \frac{1}{2}\int_0^R{\rm d}r\,r^2\int_0^{2\pi}{\rm d}\varphi\int_0^{\pi}{\rm d}\theta\ \sin\theta\,\rho(r,\theta,\varphi)\,\Phi(r,\theta,\varphi), \quad \text{(A12)}$$

which, from equations (A4)–(A5) and given the null spherical average of $\delta\rho$ and $\delta\Phi$, can be rewritten as

$$\begin{aligned} W(R) &= 2\pi\int_0^R{\rm d}r\,r^2[\langle\rho\rangle(r)\,\langle\Phi\rangle(r)+\langle\delta\rho\,\delta\Phi\rangle] \\ &= -4\pi\int_0^R{\rm d}r\,r^2\langle\rho\rangle(r)\frac{GM(r)}{r}+2\pi\int_0^R{\rm d}r\,r^2\langle\delta\rho\,\delta\Phi\rangle \\ &\equiv \mathcal{W}(R)+\delta W(R)\,, \end{aligned} \quad \text{(A13)}$$

where we have introduced the "spherical" potential energy of the truncated sphere of radius R, $\mathcal{W}$ and its difference from $W(R)$. The second equality in equation (A13) follows from partial integration of the first term on the right of the first equality, then application of the relation (A7), and one new partial integration. The resulting expression also assumes the origin of the spherically averaged potential chosen so to have

$$\langle\Phi\rangle(R)=-\frac{GM(R)}{R}\,. \quad \text{(A14)}$$

(For a spherical system truncated at R, this is equivalent to adopt the origin of $\langle\Phi\rangle(r)$ at infinity.)

Similarly, the total energy, $E=K+W$, takes the form

$$\begin{aligned} E(R) &= 4\pi\int_0^R{\rm d}r\,r^2\left\{\langle\rho\rangle(r)\left[\frac{\sigma^2(r)}{2}+\langle\Phi\rangle(r)\right]+\langle\delta\rho\,\delta\Phi\rangle\right\} \\ &= 4\pi\int_0^R{\rm d}r\,r^2\langle\rho\rangle(r)\left[\frac{\sigma^2(r)}{2}-\frac{GM(r)}{r}\right] \\ &\quad +2\pi\int_0^R{\rm d}r\,r^2\langle\delta\rho\,\delta\Phi\rangle(r)\equiv\mathcal{E}(R)+\delta\mathcal{E}(R)\,, \end{aligned} \quad \text{(A15)}$$

where we have introduced the "spherical" total energy $\mathcal{E}(R)$ and its difference from $E(R)$. Subtracting $2W$ (eq. [A13]) on both sides of equation (A9), we arrive at

$$4\pi R^3P(R)-2E(R)=4\pi\int_0^R{\rm d}r\,r^2\langle\rho\rangle(r)\frac{GM(r)}{r}$$

$$-4\pi \int_0^R \mathrm{d}r\, r^2 \langle \delta\rho\, [2\delta\Phi + r\partial_{\rm r}(\delta\Phi)]\rangle(r) \qquad \text{(A16)}$$

with $E(r)$ given by equation (A15), which can be rewritten in the usual way for the (scalar) virial relation

$$4\pi R^3 \langle\rho\rangle(R)\sigma_{\rm r}^2(R) = 4\pi \int_0^R \mathrm{d}r\, r^2 \langle\rho\rangle(r) \left[\sigma^2(r) - \frac{GM(r)}{r}\right] - 4\pi \int_0^R \mathrm{d}r\, r^3 \langle \delta\rho\, \partial_{\rm r}(\delta\Phi)\rangle(r)\,. \qquad \text{(A17)}$$

Given that the density fluctuation over the sphere, $\delta\rho$, can never be smaller than $-\langle\rho\rangle$, we have $|\delta\rho|/\langle\rho\rangle < 1$. Below we derive the exact relationship between the density fluctuation and the potential fluctuation over spheres of given radius, which shows that, unless the absolute value of the logarithmic derivative of $\delta\Phi/\langle\Phi\rangle$ is much larger than $|\delta\Phi/\langle\Phi\rangle|$ itself, which seems quite unlikely, we must also have $|\delta\Phi/\langle\Phi\rangle| < 1$. Therefore, neglecting second order terms in those deviations from sphericity, the potential and total energies given in equations (A13) and (A15) take the same form as in spherically symmetric systems,

$$W(R) \approx 4\pi \int_0^R \mathrm{d}r\, r^2 \langle\rho\rangle(r)\, \langle\Phi\rangle(r) \qquad \text{(A18)}$$

and

$$E(R) \approx 4\pi \int_0^R \mathrm{d}r\, r^2\, \langle\rho\rangle(r) \left[\frac{\sigma^2(r)}{2} - \frac{GM(r)}{r}\right], \qquad \text{(A19)}$$

by just replacing the radial profiles by their spherical averages. And the same is true for the potential energy $\widetilde{W}$ of the homogeneous toy ellipsoid mentioned in Appendix B. Despite all, for the sake of accuracy, we do not neglect in that appendix those (normally small) terms; we just make use of the fact that the spherical gravitational and total energies, $\mathcal{W}(R)$ and $\mathcal{E}(R)$, are both negative, which is guaranteed by the fact that, in steady objects, $W(R)$ and $E(R)$ are necessarily negative and that they are well-approximated at leading order by their spherical counterparts according to the relations (A18) and (A19) above.

The exact relationship between $\delta\rho/\langle\rho\rangle$ and $\delta\Phi/\langle\Phi\rangle$ can be derived taking into account that, by splitting the density and the potential given in equations (A4) and (A5), the Poisson equation takes the form

$$\Delta\left[\langle\Phi\rangle\left(1 + \frac{\delta\Phi}{\langle\Phi\rangle}\right)\right] = -4\pi G\langle\rho\rangle\left(1 + \frac{\delta\rho}{\langle\rho\rangle}\right). \qquad \text{(A20)}$$

Developing the member on the left and taking into account that, according to equation (A7), $\langle\Phi\rangle$ satisfies the Poisson equation for the spherically averaged density $\langle\rho\rangle$, making use of the relation (23), we arrive after some algebra at the exact expression

$$\left[1 + \frac{\delta\rho}{\langle\rho\rangle}(r)\right] = \left[1 + \frac{\delta\Phi}{\langle\Phi\rangle}(r)\right] \times \left[1 - \xi(r) r \frac{2\frac{\partial}{\partial r}\left(\frac{\delta\Phi}{\langle\Phi\rangle}\right) + \zeta(r) r \Delta\left(\frac{\delta\Phi}{\langle\Phi\rangle}\right)}{1 + \frac{\delta\Phi}{\langle\Phi\rangle(r)}}\right], \qquad \text{(A21)}$$

implying

$$\frac{\delta\rho}{\langle\rho\rangle}(r) = \frac{\delta\Phi}{\langle\Phi\rangle}(r) - 2\xi(r) r \frac{\partial}{\partial r}\left(\frac{\delta\Phi}{\langle\Phi\rangle}\right) - \xi(r)\zeta(r) r^2 \Delta\left(\frac{\delta\Phi}{\langle\Phi\rangle}\right), \qquad \text{(A22)}$$

where we have defined the dimensionless functions $\xi(r) = \bar{\rho}(r)/[3\langle\rho\rangle(r)] = (\mathrm{d}\ln M/\mathrm{d}R_{\rm x})^{-1}$ and $\zeta(r) = \langle\Phi\rangle(r) r/[GM(r)] = -(\mathrm{d}\ln|\langle\Phi\rangle|/\mathrm{d}\ln r)^{-1}$.

APPENDIX B: VIRIAL RADIUS IN TRIAXIAL SYSTEMS

Consider a triaxial system undergoing PA. As during virialisation ellipsoids lose energy and contract, the spherical energy $\mathcal{E}(M)$ of the truncated sphere of radius R encompassing identical mass M in the final triaxial steady object will necessarily be smaller than $\mathcal{E}_{\rm ta}(M)$ and R smaller than $R_{\rm ta}$.

Neglecting any energy exchange during virialisation across the instantaneous ellipsoid currently at turnaround (see sec. 2.2), the total energy of the system within it is preserved by taking all inner ellipsoids frozen at their respective turnaround. Suppose we evolve virtually[9] the system from such an ideal configuration by simultaneously contracting and varying the ellipticity of all the ellipsoids within the current turnaround just as their respective *apocentres* do during the virialisation of the real system. Owing to the inside-out growth of the virialised system, we can stop that virtual contraction when the total mass inside the sphere of radius R becomes equal to M, which will take place at the same time that the mass inside every inner sphere of radius r becomes also equal to the mass found inside the corresponding sphere in the real virialised ellipsoid. The spherically averaged density profile and, hence, the total mass of such a non-steady toy object will be identical, by construction, to those of the real steady object. The total energy in the truncated spheres of radius r will differ, however, from the real energy $E(r)$ because part of the energy exchange among crossing shells taking place over the real evolution of the system does not take place in the virtual evolution. Note that, in this virtual evolution, there is still some energy exchange among ellipsoids owing to their varying mass distribution, an effect which is absent in the spherically symmetric case. But as this effect is only due to the ellipticity of the system, by neglecting its ellipticity, the total energy in the truncated spheres should be conserved. In other words, the "spherical" energy defined in Appendix A for every truncated sphere, $\mathcal{E}(r)$, should be equal to that of the corresponding sphere at turnaround, $\mathcal{E}_{\rm ta}[M(r)]$.

Given that the relationship between the "spherical" potential and total energies inside truncated spheres (see App. A) is identical to that satisfied by their ordinary counterparts in spherically symmetric systems, the same proof given in Appendix C of Paper I shows that, for an homogeneous triaxial object, the spherical potential energy $\widetilde{\mathcal{W}}(R)$ for the sphere of radius R is smaller than $\mathcal{E}_{\rm ta}(M)$. It should therefore be possible to homogenise the non-steady toy ellipsoid so to end up with a uniform density equal to the mean

[9] By virtual motion we mean, as usual, any motion consistent with all the forces applied to the system, and hence, preserving its mass, energy and angular momentum, although in a way disconnected from the real dynamical timing of the system.

density of the real steady ellipsoid or the mean density $\bar{\rho}(R)$ within the associated sphere of radius R without changing its spherical total energy $\mathcal{E}_{\rm ta}(M)$ and still have a positive total kinetic energy $\mathcal{E}_{\rm ta}(M) - \widetilde{\mathcal{W}}(R)$. From that point on, we can follow exactly the same steps as in Appendix B of Paper I, that is, we can redistribute the extra kinetic energy over the homogeneous toy ellipsoid in any arbitrary homologous triaxial way compatible with the global shape of the ellipsoid, interpret the local kinetic energy so obtained as arising from some local velocity dispersion and introduce at each radius r a radial velocity dispersion $\widetilde{\sigma}_{\rm r}(r)$ according to equation (A8) for the total velocity dispersion at the radius r, $\widetilde{\sigma}(r)$, and the uniform density $\bar{\rho}(R)$. By doing this, the equilibrium equation will be satisfied at every point within such an homogeneous toy ellipsoid, which will therefore become a steady ellipsoid with uniform density equal to $\bar{\rho}(R)$ and a mass and spherical total energy within the truncated sphere of radius R respectively equal to M and $\mathcal{E}_{\rm ta}(M)$.

Consequently, $R_{\rm vir}$ given by equation (9), with $\mathcal{S}$ replaced by the spherical surface term $\widetilde{\mathcal{S}}$ arising from the new radial velocity dispersion $\widetilde{\sigma}_{\rm r}$ instead of the real one $\sigma_{\rm r}$ and the new ellipticity of the object instead of the real one, coincides accurately with the radius R of the sphere encompassing the mass M in the steady toy ellipsoid. Moreover, following exactly the same proof as in Appendix C of Paper I, but replacing W, $\widetilde{W}$ and $E_{\rm ta}$ by $\mathcal{W}$, $\widetilde{\mathcal{W}}$ and $\mathcal{E}_{\rm ta}$, it can be shown that $\widetilde{\mathcal{S}}$ coincides with $\mathcal{S}$, so there is strictly no difference between both expressions. In other words, $R_{\rm vir}$ given by equation (9) is exactly equal to R in triaxial systems just as in spherically symmetric ones.

APPENDIX C: MEAN ANGULAR MOMENTUM AND SPECIFIC VARIANCE IN TRIAXIAL SYSTEMS

The derivation followed in Appendix A of Paper III does not depend on the particular symmetry of the system, so we can start from equations (A3) and (A4) in that paper,

$$\mathrm{d}\mathbf{J}(r) = \mathrm{d}r\, 4\pi\, r^2\, \rho(r)\, \langle \mathbf{r} \times \mathbf{v} \rangle(r) = \mathrm{d}r\, 4\pi\, r^2\, \rho(r)\, \mathbf{j}(r) \qquad \text{(C1)}$$

$$\mathrm{d}V(r) = \mathrm{d}r\, 4\pi\, r^4\, \rho(r)\, \frac{\langle v_{\rm t}^2 \rangle(r)}{2} = \mathrm{d}r\, 4\pi\, r^4\, \rho(r)\, \sigma_{\rm t}^2(r)\,. \qquad \text{(C2)}$$

The integral of those two equations over a virialised triaxial object truncated at the radius R yields the total angular momentum and angular momentum variance of the system up to that radius. The modulus J of the total angular momentum vector inside r can be written in terms of the modulus l of the local specific one as

$$J(R) = \int_0^R \mathrm{d}r\, r^2 \int_0^{2\pi} \mathrm{d}\varphi \int_0^{\pi} \mathrm{d}\theta\, \sin\theta\, l(r,\theta,\varphi)\, \rho(r,\theta,\varphi)\,. \qquad \text{(C3)}$$

Thus, using the spherical average profile,

$$\langle j \rangle(r) = \frac{1}{4\pi \langle \rho \rangle(r)} \int_0^{2\pi} \mathrm{d}\varphi \int_0^{\pi} \mathrm{d}\theta\, \sin\theta\, l(r,\theta,\varphi) \rho(r,\theta,\varphi), \qquad \text{(C4)}$$

it again takes the same form as for spherically symmetric systems,

$$J(R) = 4\pi \int_0^R \mathrm{d}r\; r^2\, \langle j \rangle(r)\, \langle \rho \rangle(r)\,. \qquad \text{(C5)}$$

Similarly, the specific variance takes the form

$$V(R) = \int_0^R \mathrm{d}r\, r^4 \int_0^{2\pi} \mathrm{d}\varphi \int_0^{\pi} \mathrm{d}\theta\, \sin\theta\, v_{\rm t}^2(r,\theta,\varphi)\, \rho(r,\theta,\varphi) \qquad \text{(C6)}$$

and using the definition for the velocity dispersion in the infinitesimal spherical shell at r

$$\sigma^2(r) = \frac{1}{4\pi \langle \rho \rangle(r)} \int_0^{2\pi} \mathrm{d}\varphi \int_0^{\pi} \mathrm{d}\theta\, \sin\theta\, v_{\rm t}^2(r,\theta,\varphi) \rho(r,\theta,\varphi), \qquad \text{(C7)}$$

we arrive once again at the same form as for spherically symmetric systems

$$V(R) = 4\pi \int_0^R \mathrm{d}r\; r^2\, \sigma_{\rm t}^2(r)\, \langle \rho \rangle(r)\,. \qquad \text{(C8)}$$

APPENDIX D: ECCENTRICITIES AND MEAN SQUARED FLUCTUATIONS OVER SPHERES

Given a triaxial ellipsoid with semiaxes $a \geqslant b \geqslant c$, we define the radius R of its associated sphere as,

$$R = \left[\frac{1}{3} \left(a^2 + b^2 + c^2 \right) \right]^{1/2}\,. \qquad \text{(D1)}$$

This is not to mix up with the radius $R_{\rm e}$ of the so-called equivalent sphere, defined as

$$R_{\rm e} = (abc)^{1/3}\,. \qquad \text{(D2)}$$

Both radii coincide for spherically symmetric systems where they recover the actual radius of the object. But, while the equivalent sphere has the same volume as the ellipsoid, the associated sphere has identical mass.

To see this, consider the ellipsoidal isodensity contours $\rho_{\rm iso}(r)$ with r the radius of their associated spheres oriented in such a way that the a semiaxis is aligned with the z axis. The local density at an arbitrary point (r,θ,φ) then takes the form

$$\rho(r,\theta,\varphi) = \rho_{\rm iso}(r) \left[1 - \frac{e_{\rm p}^2(r) + e_{\rm s}^2(r)}{3} \right] \times \left[\sin^2\theta \cos^2\phi + \frac{\sin^2\theta \sin^2\phi}{1 - e_{\rm sp}^2(r)} + \frac{\cos^2\theta}{1 - e_{\rm ps}^2(r)} \right], \qquad \text{(D3)}$$

where $e_{\rm ps}$ stands either for $e_{\rm p}$ or $e_{\rm s}$ and $e_{\rm sp}$ for the alternate eccentricity. The spherically averaged density at $r = R$ is

$$\langle \rho \rangle(R) = \frac{\rho_{\rm iso}(R)}{3} \left[1 - \frac{e_{\rm p}^2(R) + e_{\rm s}^2(R)}{3} \right] G[e_{\rm p}^2(R), e_{\rm s}^2(R)]\,, \qquad \text{(D4)}$$

where

$$G[e_{\rm p}^2(R), e_{\rm s}^2(R)] \equiv \left[1 + \frac{1}{1 - e_{\rm s}^2(R)} + \frac{1}{1 - e_{\rm p}^2(R)} \right]\,. \qquad \text{(D5)}$$

Thus, the mass within the sphere of radius R associated with the ellipsoid of semiaxes $a(R)$, $b(R)$ and $c(R)$, given by

$$M(R) = \int_0^{\pi} \mathrm{d}\theta \sin\theta \int_0^{2\pi} \mathrm{d}\phi \int_0^R \mathrm{d}r\, r^2\, \rho(r,\theta,\varphi)\,, \qquad \text{(D6)}$$

takes, according to equation (D4), the form

$$M(R) = 4\pi \int_0^R \mathrm{d}r\, r^2\, \langle \rho \rangle(r)\,, \qquad \text{(D7)}$$

which implies that the mass of the ellipsoid is equal, indeed, to the mass of the sphere with radius R.

We can now calculate the rms density fluctuation over the sphere of radius r. Dividing equation (D3) by $\langle\rho\rangle(r)$ and replacing $\rho_{\rm iso}(r)$ by its value given in equation (D4), we obtain

$$1+\frac{\delta\rho}{\langle\rho\rangle}(r,\theta,\phi)=3\,G^{-1}[e_{\rm p}^2(r),e_{\rm s}^2(r)] \times\left[\sin^2\theta\cos^2\phi+\frac{\sin^2\theta\sin^2\phi}{1-e_{\rm sp}^2(r)}+\frac{\cos^2\theta}{1-e_{\rm ps}^2(r)}\right]. \quad \text{(D8)}$$

The squared density fluctuation over the sphere of radius r can be readily determined by computing

$$\left\langle\left(\frac{\delta\rho}{\langle\rho\rangle}\right)^2\right\rangle(r)=\frac{1}{4\pi}\int_0^{\pi}{\rm d}\theta\sin\theta\int_0^{2\pi}{\rm d}\phi\left(\frac{\delta\rho}{\langle\rho\rangle}\right)^2(r,\theta,\phi), \quad \text{(D9)}$$

with $\delta\rho/\langle\rho\rangle$ given by equation (D8). The result is equation (41).

The rms density fluctuation over the sphere associated with a given ellipsoid (eq. [D9]) can be related to the quantity (see eq. [A15])

$$\left\langle\frac{\delta\rho}{\langle\rho\rangle}\frac{\delta\Phi}{\langle\Phi\rangle}\right\rangle(r)=\frac{1}{4\pi r^2\langle\rho\rangle(r)\langle\Phi\rangle(r)}\frac{{\rm d}(\delta\mathcal{E})}{{\rm d}r}, \quad \text{(D10)}$$

through the relation (A21) arising from the Poisson equation. For this to be possible we need the full characterisation of $\delta\rho(r,\theta,\varphi)$, which unfortunately is unknown for peaks. We will assume here that the ellipsoids both in protoobjects and virialised objects have rms dimensionless density fluctuation profiles of the power-law form with index κ, $\langle(\delta\rho/\langle\rho\rangle)^2\rangle^{1/2}=Qr^{\kappa}$, which is equivalent for non-rotating axes[10] to assume $\partial[\delta\rho(r,\theta,\varphi)/\langle\rho\rangle(r)]/\partial r=\kappa Ar^{\kappa-1}$

Multiplying equation (A22) by the dimensionless density fluctuation, averaging over the sphere of radius r and taking into account the divergence theorem, we are led to

$$\left\langle\left(\frac{\delta\rho}{\langle\rho\rangle}\right)^2\right\rangle(r)=G(r)\left\langle\frac{\delta\rho}{\langle\rho\rangle}\frac{\delta\Phi}{\langle\Phi\rangle}\right\rangle(r)-\xi(r)\zeta(r)\,r^2 \times\left\{\frac{2\,[1+(1-\kappa)\zeta(r)]}{\zeta(r)r}\frac{\rm d}{{\rm d}r}\left\langle\frac{\delta\rho}{\langle\rho\rangle}\frac{\delta\Phi}{\langle\Phi\rangle}\right\rangle+\frac{{\rm d}^2}{{\rm d}r^2}\left\langle\frac{\delta\rho}{\langle\rho\rangle}\frac{\delta\Phi}{\langle\Phi\rangle}\right\rangle\right\} \quad \text{(D11)}$$

with $G(r)\equiv 1+\kappa\xi(r)[2+(1-\kappa)\zeta(r)]$. Equation (D11) is an ordinary differential equation that can be solved for the mean dimensionless density-potential crossed fluctuation given the mean squared density fluctuation (the boundary conditions are set by trivial consistency conditions at $r=0$).

On the other hand, multiplying equation (A22) by the dimensionless potential fluctuation, a similar derivation as above leads to

$$\left\langle\frac{\delta\rho}{\langle\rho\rangle}\frac{\delta\Phi}{\langle\Phi\rangle}\right\rangle(r)=\left\langle\left(\frac{\delta\Phi}{\langle\Phi\rangle}\right)^2\right\rangle(r)-\xi(r)\zeta(r)r^2 \times\left\{\frac{2[1+\zeta(r)]}{\zeta(r)r}\frac{\rm d}{{\rm d}r}\left\langle\left(\frac{\delta\Phi}{\langle\Phi\rangle}\right)^2\right\rangle+\frac{{\rm d}^2}{{\rm d}r^2}\left\langle\left(\frac{\delta\Phi}{\langle\Phi\rangle}\right)^2\right\rangle -\left\langle\left(\frac{\partial}{\partial r}\frac{\delta\Phi}{\langle\Phi\rangle}\right)^2\right\rangle\right\}. \quad \text{(D12)}$$

Equation (D12) with trivial boundary conditions at $r=0$ cannot yet be solved for the mean squared potential fluctuation because of the presence of the unknown mean squared derivative of the dimensionless potential (the last term on the right). To solve this drawback we must multiply equation (A22) by the partial derivative of the dimensionless potential fluctuation and, operating as usual, we arrive at

$$\frac{\rm d}{{\rm d}r}\left\langle\frac{\delta\rho}{\langle\rho\rangle}\frac{\delta\Phi}{\langle\Phi\rangle}\right\rangle-\frac{\kappa}{r}\left\langle\frac{\delta\rho}{\langle\rho\rangle}\frac{\delta\Phi}{\langle\Phi\rangle}\right\rangle(r)=\frac{1}{2}\frac{\rm d}{{\rm d}r}\left\langle\left(\frac{\delta\Phi}{\langle\Phi\rangle}\right)^2\right\rangle -\xi(r)\zeta(r)r\left\{\frac{2\,[1+\zeta(r)]}{\zeta(r)}\left\langle\left(\frac{\partial}{\partial r}\frac{\delta\Phi}{\langle\Phi\rangle}\right)^2\right\rangle(r) +\frac{1}{2}\frac{\rm d}{{\rm d}r}\left\langle\left(\frac{\partial}{\partial r}\frac{\delta\Phi}{\langle\Phi\rangle}\right)^2\right\rangle\right\}. \quad \text{(D13)}$$

Replacing into equation (D13) the mean squared partial derivative of the dimensionless potential given by equation (D12) and its radial derivative drawn from the differentiation of the same equation, we finally obtain

$$\left\langle\frac{\delta\rho}{\langle\rho\rangle}\frac{\delta\Phi}{\langle\Phi\rangle}\right\rangle(r)+\frac{3\,r}{4\widetilde{I}(r)}\frac{\rm d}{{\rm d}r}\left\langle\frac{\delta\rho}{\langle\rho\rangle}\frac{\delta\Phi}{\langle\Phi\rangle}\right\rangle=\frac{I(r)}{\widetilde{I}(r)}\left\langle\left(\frac{\delta\Phi}{\langle\Phi\rangle}\right)^2\right\rangle(r) -\frac{3\xi(r)r}{4\widetilde{I}(r)}\left\{H(r)\frac{\rm d}{{\rm d}r}\left\langle\left(\frac{\delta\Phi}{\langle\Phi\rangle}\right)^2\right\rangle+[1+\zeta(r)]r \times\frac{{\rm d}^2}{{\rm d}r^2}\left\langle\left(\frac{\delta\Phi}{\langle\Phi\rangle}\right)^2\right\rangle+\frac{\zeta(r)r^2}{6}\frac{{\rm d}^3}{{\rm d}r^3}\left\langle\left(\frac{\delta\Phi}{\langle\Phi\rangle}\right)^2\right\rangle\right\}, \quad \text{(D14)}$$

with

$$H(r)\equiv\frac{1}{3}\left[4I(r)+3\zeta(r)-2\xi^{-1}(r)+\frac{{\rm d}\ln\xi}{{\rm d}\ln r}+5\right], \quad \text{(D15)}$$

$$I(r)\equiv 1+\zeta^{-1}(r)+\frac{1}{4}\frac{{\rm d}\ln}{{\rm d}\ln r}\left(\frac{\zeta}{\xi\,r^2}\right) \quad \text{(D16)}$$

and $\widetilde{I}(r)=I(r)-\kappa/2$. Equation (D14) with trivial boundary conditions at $r=0$ can then be solved for the mean squared dimensionless potential fluctuation. Note that the mean dimensionless $\delta\rho\,\partial_r\delta\Phi$ fluctuation profile entering the Jeans equation for anisotropic spherically averaged triaxial systems (eq. [A8]) can be readily inferred from the radial derivative of the mean density potential crossed fluctuation.

One particular case is that of homologous ellipsoids, $\kappa=0$. Equations (D11), (D12) and (D14) then have the trivial solutions,

$$\left\langle\frac{\delta\rho}{\langle\rho\rangle}\frac{\delta\Phi}{\langle\Phi\rangle}\right\rangle(r)=\left\langle\left(\frac{\delta\Phi}{\langle\Phi\rangle}\right)^2\right\rangle(r) =\left\langle\left(\frac{\delta\rho}{\langle\rho\rangle}\right)^2\right\rangle(r)=Q\,, \quad \text{(D17)}$$

both for the protoobject at turnaround and the virialised object (see eq. [39]). This approximation is not valid for haloes

[10] This can be seen taking into account that, as $\langle\delta\rho/\langle\rho\rangle\rangle=0$, either the integral of $\delta\rho(r,\theta,\varphi)/\langle\rho\rangle(r)$ over ϕ is an even function of θ or the integral of $\sin(\theta)\delta\rho(r,\theta,\varphi)/\langle\rho\rangle(r)$ over θ is an odd function of ϕ and that the condition $\langle(\delta\rho/\langle\rho\rangle)^2\rangle^{1/2}=Qr^{\kappa}$ implies the contrary relation for $\{\partial[\delta\rho(r,\theta,\varphi)/\langle\rho\rangle(r)]/\partial r\}-k[\delta\rho(r,\theta,\varphi)/\langle\rho\rangle(r)]/r$.

and peaks simultaneously over the whole radial range. However, it is valid close enough to the origin of the respective objects. To see this, we must relate the final mean squared density fluctuation directly to the initial one. Taking into account equations (40) and (41) and the condition (A14) both at turnaround and in the virialised object, we arrive at

$$U(R)\left\langle\left(\frac{\delta\rho}{\langle\rho\rangle}\right)^2\right\rangle(R)=\left\langle\left(\frac{\delta\rho_{\rm ta}}{\langle\rho_{\rm ta}\rangle}\right)^2\right\rangle(R_{\rm ta})\,, \tag{D18}$$

with $U(R)$ given by equation (43) with $\kappa\gamma = 0$, that is $U(R) = C(R)/D(R)$. As the mean squared fluctuations on both sides of equation (D18) are constant and equal to Q, this implies that $C(r)/D(r)$ must also be constant. For the typical NFW (or Einasto) $\langle\rho\rangle(r)$ profile and the typical mass-concentration relation this is roughly satisfied, indeed, with a value of that ratio between one and two.

To solve equations (38) and (42) it is convenient to change the variables $e_{\rm p}$ and $e_{\rm s}$ into the quantities $R_{\rm e}/R$ and $R_{\rm e}/a$. From the definition of the eccentricities (eqs. [34] and [35]) and their relationships to R and $R_{\rm e}$ (eqs. [D1] and [D2]), we have

$$\left(\frac{R_{\rm e}}{a}\right)^6=(1-e_{\rm p}^2)(1-e_{\rm s}^2) \tag{D19}$$

$$\left(\frac{R_{\rm e}}{R}\right)^6=27\,\frac{(1-e_{\rm p}^2)(1-e_{\rm s}^2)}{[1+(1-e_{\rm p}^2)+(1-e_{\rm s}^2)]^3}\,, \tag{D20}$$

which can be inverted by first solving the biquadratic equation

$$e_{\rm s}^4-3\left(1-\frac{R^2}{R_{\rm e}^2}\frac{R_{\rm e}^2}{a^2}\right)e_{\rm s}^2-\frac{R_{\rm e}^2}{a^2}\left(3\frac{R^2}{R_{\rm e}^2}-\frac{R_{\rm e}^4}{a^4}\right)+2=0\,, \tag{D21}$$

and then replacing the solution into the equation

$$e_{\rm p}^2=3\left(1-\frac{R^2}{a^2}\right)-e_{\rm s}^2\,. \tag{D22}$$

Specifically, the only one solution of the biquadratic equation (D21) guaranteeing the positiveness of the eccentricities and the condition $e_{\rm p}\geqslant e_{\rm s}$ is

$$e_{\rm p}^2=\frac{3}{2}\left(1-\frac{R^2}{R_{\rm e}^2}\frac{R_{\rm e}^2}{a^2}\right)+\left[\frac{9}{4}\left(1-\frac{R^2}{R_{\rm e}^2}\frac{R_{\rm e}^2}{a^2}\right)^2+\frac{R_{\rm e}^2}{a^2}\left(3\frac{R^2}{R_{\rm e}^2}-\frac{R_{\rm e}^4}{a^4}\right)-2\right]^{1/2} \tag{D23}$$

$$e_{\rm p}^2=\frac{3}{2}\left(1-\frac{R^2}{R_{\rm e}^2}\frac{R_{\rm e}^2}{a^2}\right)-\left[\frac{9}{4}\left(1-\frac{R^2}{R_{\rm e}^2}\frac{R_{\rm e}^2}{a^2}\right)^2+\frac{R_{\rm e}^2}{a^2}\left(3\frac{R^2}{R_{\rm e}^2}-\frac{R_{\rm e}^4}{a^4}\right)-2\right]^{1/2}. \tag{D24}$$

In the new variables, equations (38) and (41) transform into (see the relations [D19] and [D20])

$$\frac{R_{\rm e}(R)}{R}=\frac{R_{\rm e}(R_{\rm ta})}{R_{\rm ta}} \tag{D25}$$

$$\frac{R}{R_{\rm e}(R)}\frac{R_{\rm e}^4(R)}{a^4(R)}=\frac{1}{3}\left[1+\frac{5}{2}\left\langle\left(\frac{\delta\rho}{\langle\rho\rangle}\right)^2\right\rangle(R)\right]^{1/2}\times\left[\frac{R_{\rm e}^6(R)}{a(R)^6}+3\frac{R^2}{R_{\rm e}^2(R)}\frac{R_{\rm e}^2(R)}{a^2(R)}-1\right], \tag{D26}$$

which can be readily solved for the quantities $R_{\rm e}(R)/R$ and $R/a(R)$. Then, the eccentricities $e_{\rm p}(R)$ and $e_{\rm s}(R)$ can be obtained by means of equations (D23) and (D24).